Forest destruction by 'a'ā lava flow during Etna's 2002-03 eruption: Mechanical, thermal, and environmental interactions

Andrew Harris, Stefano Mannini, Laura Calabrò, Sonia Calvari, Lucia Gurioli, Magdalena Oryaëlle Chevrel, Massimiliano Favalli, Nicolas Villeneuve

Forest destruction by ‘a‘ā lava flow during Etna's 2002–03 eruption: Mechanical, thermal, and environmental interactions

Andrew Harris [a,*], Stefano Mannini [a,b], Laura Calabrò [a,c], Sonia Calvari [d], Lucia Gurioli [a], Magdalena Oryaëlle Chevrel [a], Massimiliano Favalli [e], Nicolas Villeneuve [f]

[a] Université Clermont Auvergne, CNRS, IRD, OPGC, Laboratoire Magmas et Volcans, 63000 Clermont-Ferrand, France
[b] Department of Earth Sciences, University of Geneva, Geneva, Switzerland
[c] Department of Geological Science, University of Roma Tre, Roma, Italy
[d] Istituto Nazionale di Geofisica e Vulcanologia, Osservatorio Etneo – Sezione di Catania, Piazza Roma 2, Catania 95125, Italy
[e] Istituto Nazionale di Geofisica e Vulcanologia – Sezione di Pisa, Via Cesare Battisti 53, Pisa 56125, Italy
[f] Institut de Physique du Globe Paris, 1 Rue Jussieu, 75005 Paris, France

ARTICLE INFO

Keywords:
Channelized ‘a‘ā lava flow
Forest interaction
Tree molds
Cooling rates
Phenocrysts

ABSTRACT

Forest destruction by ‘a‘ā lava flow is common. However, mechanical and thermal interactions between the invading lava and the invaded forest are poorly constrained. We complete mapping, thermal image and sample analyses of a channel-fed ‘a‘ā lava flow system that invaded forest on the NE flank of Mt. Etna (Italy) in 2002. These lava flows destroyed 231,000 trees, only 2% of which are still visible as felled trunks on the levees or at the channel-levee contact. The remaining 98% were first felled by the flow front, with the trunks then buried by the flow. Rare tree molds can be found at the rubble levee base where trees were buried by avalanching hot breccia and then burnt through, with a time scale for total combustion being a few days. Protruding trunks fell away from the flow, if felled by blocks avalanching down the levee flank, or became aligned with the flow if falling onto the moving stream. Estimated cooling rates (0.1–5.5 °C km^{-1}) are normal for well-insulated ‘a‘ā flow, suggesting no thermal interaction. We find the highest phenocryst concentrations (of 50–60%, above an expected value of 30–40%) in low velocity (<0.5 m s^{-1}) locations. These low velocity zones are also characterized by high trunk concentrations. Thus, the common factor behind crystal and trunk deposition is velocity. That is, when the lava slows down, crystal settling occurs and trunks are preferentially deposited. Thus, although we find no thermal or textural effects due to the presence of the forest, we do find mechanical and environmental interactions where the trees are consumed to become part of the flow.

1. Introduction

Forest destruction by lava flow ingress is a common phenomenon that occurs at many effusive centers. This includes all frequently active effusive sites such as Kīlauea, e.g., during the July 1974 eruption (Lockwood et al., 1999), Piton de la Fournaise, e.g., during the 1986 eruption (Bertile, 1987) and Etna, e.g., during the 1974 west flank eruption (Lormand et al., 2020). For pāhoehoe lava flowing around a tree, if the lava level drops during the interaction, a lava tree can form; this being an upstanding column of solidified lava surrounding a cylindrical void left by the burnt-away tree (Finch, 1931; Macdonald et al., 1983). A tree mold, however, can form if the lava level remains constant, this being a “hollow cylinder” (Moore and Richter, 1962) or “hole” (Finch, 1931) in the solidified lava marking the location of the burnt-away tree trunk. Lava tree and tree mold formation in pāhoehoe is a well-known process (e.g., Finch, 1931; Moore and Richter, 1962; Lockwood and Hazlett, 2010; Jones et al., 2017). As a result, interest has focused on the interaction of pāhoehoe and trees to form such structures (e.g., Carveni et al., 2011; Lockwood and Williams, 1978; Moore and Richter, 1962) and the resulting mechanical and thermal interactions with the surrouding lava (Biren et al., 2020; Chevrel et al., 2019). Lava trees and tree molds in pāhoehoe can in turn be used to infer flow direction (Lockwood and Williams, 1978), measure flow thickness (Moore and Kachadoorian, 1980; Moore and Richter, 1962) and to reconstruct pre-eruption topography (Jones et al., 2017; Parcheta et al., 2012). However, less attention has been focused on the nature of

* Corresponding author.
E-mail address: andrew.harris@uca.fr (A. Harris).

https://doi.org/10.1016/j.jvolgeores.2022.107621

environmental, mechanical, and thermal interactions between trees and surrounding lava during ‘a‘ā flow emplacement. In fact, almost no study has been made of the interaction between ‘a‘ā lava flows and a forest, and/or how orientations of trees in ‘a‘ā can be used to retrieve flow dynamics.

Chevrel et al. (2019) observed that lava trees can only be formed when the lava flow is fluid enough. When the lava becomes too viscous, trees will be overridden and no lava tree can be formed, so that lava trees tend to be absent in ‘a‘ā flow domains. Although Chevrel et al. (2019) found no signs of enhanced cooling down a pāhoehoe flow due to the presence of the trees, Biren et al. (2020) found evidence for enhanced cooling and crystallization, as well as chemical interactions, in the rind of quenched lava around a tree mold forming in pāhoehoe. However, the physical interactions between an ‘a‘ā lava flow and trees remain largely undefined and unexamined. We aim to fill this gap by examining the mechanical, thermal and environmental interactions between ‘a‘ā lava and trees focusing on Etna's 2002–03 eruption.

During Etna's 2002–03 eruption, an ‘a‘ā lava flow fed by a fissure active on the N-NE flank advanced 7 km through coniferous and mixed woodland, destroying about 2 km^2 of the Linguaglossa Pine Forest and the ski station of Piano Provenzana (Fig. 1). We use a combination of thermal images acquired during the eruption and high spatial resolution digital imagery, in tandem with field mapping and sampling, to define heat losses and cooling down this flow. We also use mapping of felled tree location and orientation, plus field measurements of tree location and survival, to define the nature of the ‘a‘ā-forest interaction. We find normal conditions for down-flow cooling and crystallization, but are able to define a mechanical effect where the trees become a component of the lateral levees and basal crust. We find rare lava tree molds but no lava trees, the interaction being almost entirely destructive. However, we can use the orientation of tree trunks surviving on the flow surface to reconstruct flow direction and interaction mode.

2. The 2002–03 Etna eruption and the “*Linguaglossa*” flow

Between 26 and 27 October 2002, intense seismicity accompanied the opening of two eruptive fissure systems on Etna's S and NE flanks (Andronico et al., 2005, 2009). Beginning during the early hours of 27 October, a fissure system opened on the NE Rift between the elevations of 2500 and 1890 m asl (Andronico et al., 2009), where satellite-derived Time Averaged Discharge Rates (TADR; Harris et al., 2007) recorded a peak of 30–60 $m^3\ s^{-1}$ during the evening of 27 October (Harris et al., 2011, 2012). In the early morning of 28 October, a vent opened on the lowermost end of the fissure system to feed a flow which moved 2.5 km to the NE in “a few hours” (Andronico et al., 2009). During 29 October, the NE flow slowed; but a new flow moved out of the vent to the SE, invading the Piano Provenzana before turning east (Fig. 1). The NE flow stopped on 31 October, having travelled 2.8 km (Andronico et al., 2009). The main eastward-advancing flow, however, continued to advance through the forest above the town of Linguaglossa (Fig. 1), remaining active for a further four days before stopping at an elevation of 1150 m asl on 3 November having reached a final length of around 6.2 km (Andronico et al., 2009), yielding a time-averaged advance rate of 1550 m/day. We focus herein on this flow unit (highlighted on Fig. 1), which we hereafter term the “Linguaglossa” lava flow. Andronico et al. (2009) note that this Linguaglossa flow “caused fires and destroyed parts of the old Linguaglossa pine forest”, that it was ‘a‘ā in type, and contained “wide channels”. TADR recorded during its initial emplacement (29–30 October) were 20–55 $m^3\ s^{-1}$ (Harris et al., 2011, 2012).

The Linguaglossa pine forest comprises trees that are up to 115–140 years old, covers an area of 1178 ha (11.78 km^2) and is in zone B[1] of the *Parco Regionale dell'Etna* (Barreca et al., 2009, 2010). The forest is of *pinus laricio* (black pine), a tree what characterizes Etna's forests between the elevations of 1100 and 1700 m asl (Marchese, 1991). Black pines can reach 40 m in height, with trunks typically being vertical with horizontal branches and a dense, pyramidal canopy (Testi, 2003). However, the pines of the Linguaglossa forest have heights of 25–29 m, with an average of 27 m, and trunk diameters of 38.1–56.3 cm, with an average of 47.8 cm (Barreca et al., 2010). Below 1200 m asl, oaks (*quercus pubescens*) are dominant. The oaks are shorter, growing up to 15 m high (Marchese, 1991), having an average height 5 m and trunk diameter of 2 cm in the Linguaglossa forest (Barreca et al., 2010).

3. Methods

3.1. Tree mapping and sampling

Lava flow mapping and tree digitalization were carried out using Google Earth© imagery (Image © 2017 Digital Globe) and shaded relief maps derived from the 2-m spatial resolution LiDAR-derived DEM produced for Etna by Favalli et al. (2009). We used this combination of imagery to map the location of all felled trees remaining on the flow surface, as well as their length and orientation. Tree orientation (θ_3), as defined in Fig. 2, was obtained from:

$$\theta_3 = \theta_f - \theta_T \quad (1)$$

where θ_f is the flow azimuth and θ_T is the tree azimuth. In addition, during February 2017, a UAV survey allowed acquisition of high-spatial resolution imagery covering an area of 0.15 km^2. The UAV (a DJI Phantom 3) was mounted with a 12MP camera which provided 4000 × 3000 pixel images. This allowed generation of a 6-cm spatial resolution DEM and a 3-cm orthomosaic (cf. Favalli et al., 2018; Lormand et al., 2020) for a control area in the medial section of the flow field (Fig. 2) and the flow front. The orthomosaic for the medial area also allowed estimation of tree density beyond the flow field. This was obtained by measuring the mean distance between each tree, and was validated by field-based tree-counts. This involved counting all trees in two 20 × 20 m areas, at sites E02 and E10 (Fig. 1), as well as measuring the trunk diameter and perimeter. Tree density was used to estimate the expected number of trees covered by the flow and to produce ratios of accountable trees (those felled trees remaining on the flow surface) and unaccountable trees (those trees for which there is now no trace). Finally, within the medial area, we made a detailed orthophoto mosaic and DEM using a camera mounted on a 6 m high pole with red paper napkins as ground control points.

3.2. Thermo-dynamic parameters of lava flow

During the eruption, thermal images were collected by the Istituto Nazionale di Geofisica e Vulcanologia – Osservatorio Etneo (INGV-OE) during helicopter overflights and ground-based surveys. Images (as given in Fig. 3) were collected of the entire channel system from the vent, through the medial section, to the flow front using a Forward Looking Infrared Radiometer (FLIR) thermal (7.5–13 μm) camera. The camera was a ThermaCam SC660 which acquires 320 × 240 pixel images with a 24 × 18° field-of-view (FOV) and in which the pixel instantaneous field of view (IFOV) is 1.3 mrad. While pixel sizes were calculated using the distance between the camera and the target, plus the angle at which the surface was viewed (Harris, 2013), pixel-integrated temperatures were corrected for atmospheric effects by inputting emissivity, air temperature, relative humidity, and path length into the correction routine on board the camera. These images were used to estimate flow velocity, heat loss and cooling rate, as well as temperatures in fires burning in the trees and their canopies in, over and around the flow (e.g., Fig. 4).

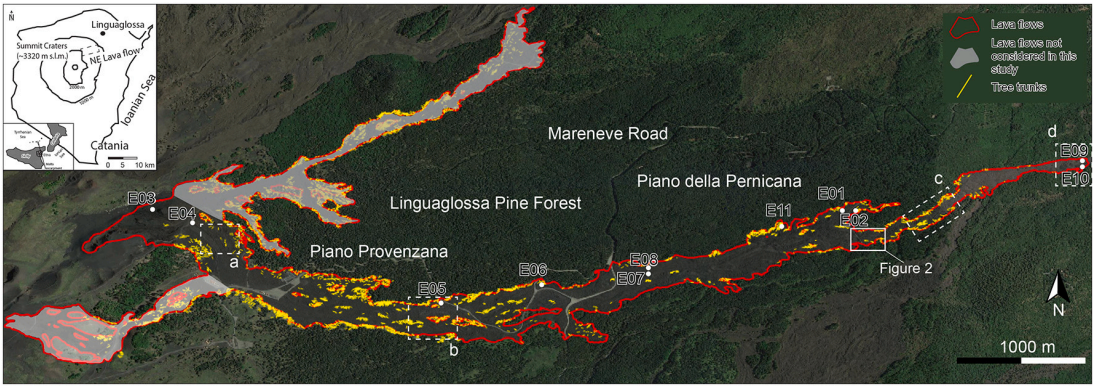

Fig. 1. Map of the 2002–2003 Linguaglossa Lava Flow field that erupted from the NE-Rift, with location inset. The red line is the limit of the flow field, the grey zones are areas not considered here, where tree trunks lying on the flow surface are given as yellow lines. Locations, orientations and lengths of all of these trees were entered into our database. Black numbers with white outline identify sample locations, solid-line white square corresponds to location of the UAV survey for which the orthomosaic is given in Fig. 2 and the dashed-line white squares correspond to locations of the thermal images given in Fig. 3 (parts a, b, c, d). Base image courtesy of Google Earth (image: Digital Globe 2017). (For interpretation of the references to colour in this figure legend, the reader is referred to the web version of this article.)

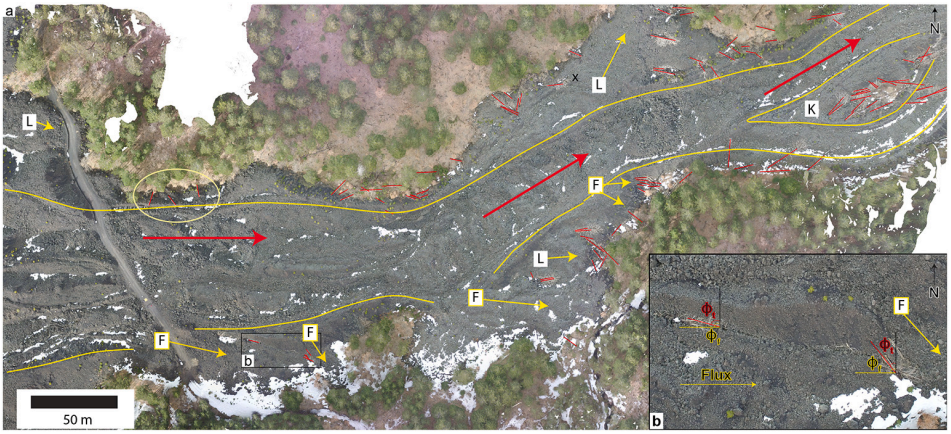

Fig. 2. Optical imagery from the UAV overflight (see Fig. 1 for location). (a) Orthomosaic (3 cm pixel resolution) made from 263 visible images using Agisoft Metashape. Red arrows mark flow direction in the main channel, and yellow lines follow the levee crests. Yellow arrows labelled "L" and "F" locate stalled lateral lobes and breakout flow from levee failure, respectively; arrow direction gives flow direction. "K" marks a kīpuka. Note alignment of tree trunk with direction of breakout at all cases marked "F" (including case magnified in inset). Instead, tree trunks surrounded by rubble levee (in the yellow ellipse) have fallen at a direction of 90° from the main flow direction. Letter "x" marks location of tree mold of Figs. 10 and 12. (b) Magnification of a zone containing two felled trees showing the flux direction (Φ_f) and tree azimuth (Φ_t). (For interpretation of the references to colour in this figure legend, the reader is referred to the web version of this article.)

3.2.1. Velocity

On 2 November a time series of images was taken of the master channel around 750 m from the vent (Fig. 3a). The distance to the near and far bank of the channel was 20 and 50 m, respectively, giving pixel sizes of 0.35 m at the near-edge of the channel and 1.68 m at the far edge. Images were collected every 5 s and velocities were obtained from the distance travelled by identifiable thermal features (cold crust and hot cracks) between sequential images. Elsewhere velocity (v) was approximated using the Jeffreys equation (Jeffreys, 1925):

$$v = \frac{h^2 \rho g \sin\vartheta}{3\mu} \tag{2}$$

Here h is the lava depth in the channel, as measured in the field at each sampling location, ϑ is the ground slope, g is acceleration due to gravity, ρ is the sample-derived lava density, and μ is viscosity. Because we were unable to collect glassy samples so as to derive flow temperatures and crystallinities (cf. Cashman et al., 1999; Riker et al., 2009; Robert et al., 2014), we were also unable to estimate the lava effective viscosity. We thus used a value of 10^4 Pa s proximally and 10^5 Pa s medially and distally, which are values typical for Etna lava (Calvari et al., 1994; Gauthier, 1973; Harris and Allen, 2008; Lormand et al., 2020; Pinkerton and Sparks, 1978; Tanguy et al., 1973; Walker, 1967).

3.2.2. Heat loss and cooling rate

Flow surface temperatures (T_s) were converted to total heat loss (Q_{Tot}) by calculating and summing radiative (Q_{Rad}) and convective (Q_{Conv}) heat losses

$$Q_{Tot} = Q_{Rad} + Q_{Conv} \tag{3}$$

$$Q_{Rad} = \varepsilon\sigma\left[(T_s)^4 - (T_a)^4\right] \tag{4}$$

$$Q_{Conv} = h_c(T_s - T_a) \tag{5}$$

in which T_a is the ambient temperature, ε is emissivity, σ is the Stefan-Boltzmann constant, and h_c is the convective heat transfer coefficient (see Appendix A for assumed values). Following Keszthelyi (1995), total heat loss and flow velocity were then used to estimate the cooling rate of the flow interior per meter advanced (dT/dx) in:

$$\frac{dT}{dx} = \frac{Q_{Tot}}{vh\rho\left(C_p + C_L\frac{d\varphi}{dT}\right)} \tag{6}$$

in which C_p is the lava specific heat capacity, ρ is the lava density, C_L is latent heat of crystallization, and $d\varphi/dT$ is the mass fraction of crystals grown per degree cooling (see Appendix A for assumed values).

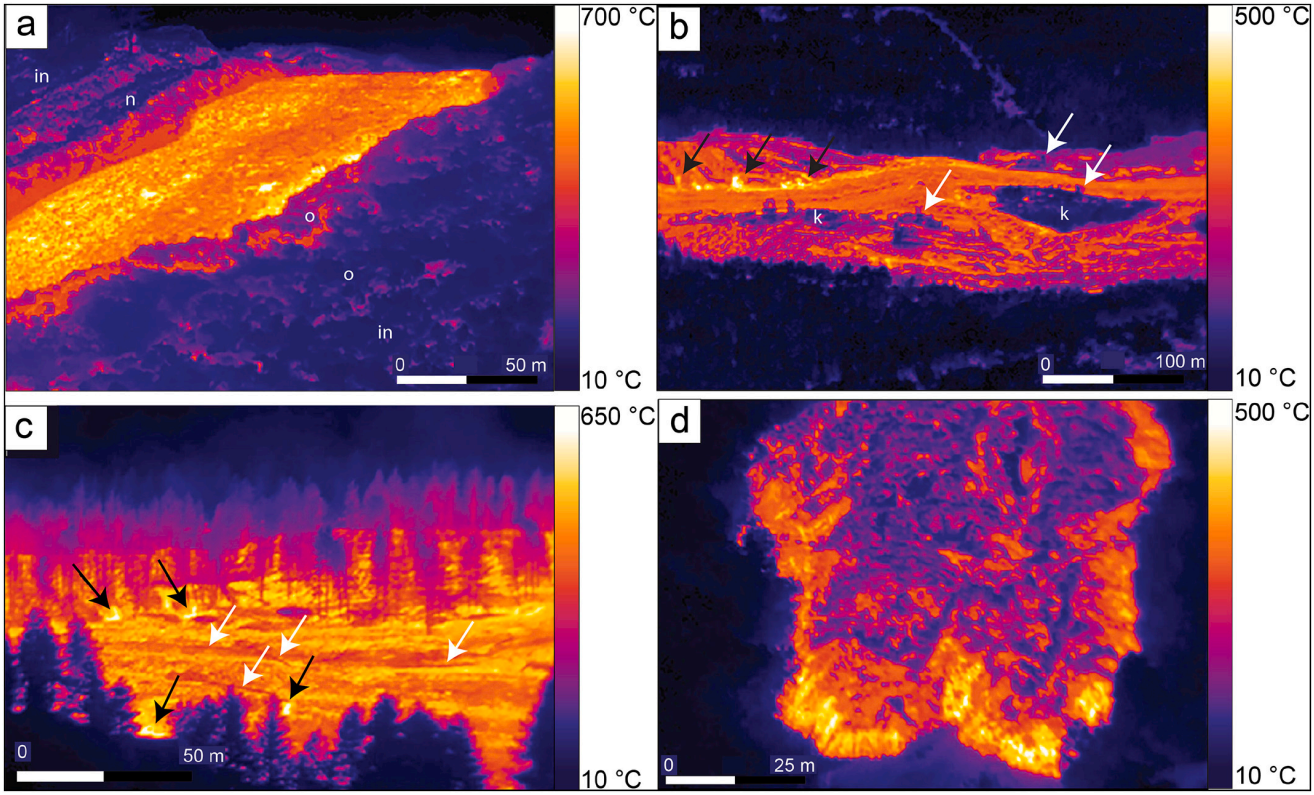

Fig. 3. Thermal images of the Lingualossa flow acquired on 27 October and 2 November 2002 (see Fig. 1 for image locations, flow direction is right to left, except for (d) in which it is top to bottom). (a) Low-oblique ground-based image acquired on 2 November at 16 h10 looking west into the master channel leaving the vent area showing the thermal structures associated with the active ʻaʻā channel. Note, the surface is generally of a high temperature, where embryonic, but hot, ʻaʻā clasts are beginning to form. Following Lipman and Banks (1987), the channel is stable in form, where the levees are static, the channel-levee boundary is distinct and the levees are compound, comprising initial ("in"), nested ("n") and overflow ("o") forms. (b) High-oblique helicopter-based image acquired 2 November at 09 h32 looking south onto the master channel in its proximal-medial reach showing trees burning at the levee-channel contact and non-burning trees still standing in and kīpukas ("k") in the braided channel (examples marked with black and white arrows, respectively). (c) Low-oblique helicopter-based image acquired 27 October at 14 h26 looking south onto the master channel in its distal-medial reach showing trees burning at the levee-channel contact and non-burning, cold, trunks floating on the flow surface and aligned with the flow direction (examples marked with black and white arrows, respectively). Note, large stands of non-burning trees surviving in the broad, still hot but stagnant, initial levee to the south. Following Lipman and Banks (1987), the channel is transitional in form, where the initial levees are beginning to form, but can still deform and the channel-levee boundary is indistinct. Note also thermal reflection on the standing trees from the active lava (indicative of a high temperature environment in which the trees are being heated and dried before combustion, cf. Biren et al. (2020)). (d) Helicopter-based near-vertical view of the flow front on 2 November at 09 h37 (west is up). Note, the surface is now well insulated with an extensive covering of large, cool, ʻaʻā clasts. Following Lipman and Banks (1987), the flow is dispersed (i.e., movement is occurring across the entire flow front) and classic forward rolling motion of the flow front is causing temperatures to be highest at the flow front due to continued crust disruption by near-continuous avalanching of surface crust down the frontal scarp (cf. Harris et al., 2002). In the nomenclature of Kilburn and Guest (1993) flow front type is "distal-type (rubbly)" where ʻaʻā with larger clinkers forms the scree through which flow front extrusions occur.

3.3. *Chemical and textural analysis*

In February 2017, we collected 10 cm-sized lava samples approximately every 0.3 km between the vent and the flow front (Fig. 1; Table 1). One bomb (at Site 1, Fig. 1; Sample E3, Table 1) was also sampled close to the vent. Extrusions of the flow interior outcropping in the levees and flow front were sampled, where samples were selected to be as glassy and unaltered as possible. However, no sample was found to be entirely glassy, excluding the possibility to analyse the glass and apply geothermometry. However, bulk rock major elements were analysed for the near-vent sample (E3) using Inductively Coupled Plasma-Atomic Emission Spectroscopy (ICP-AES) with a Jobin-Yvon Ultima-C spectrometer at the Laboratoire Magmas et Volcans (Université Clermont Auvergne, Clermont Ferrand, France). Additionally, chemical analysis on mineral phases was performed using an electron microprobe CAMECA SX 100 (at 15 KeV with a 15 nA with a spot size of 10 μm).

For textural analyses, samples were cleaned and dried in an oven at 70 °C for 24 h. Bulk densities were then acquired using the Archimedes approach following Houghton and Wilson (1989). Instead, for samples <5 cm in diameter, we used a Geopyc 1360 Envelope Density Analyzer (Thivet et al., 2020) to obtain density, and the dense rock equivalent (DRE) density was determined from the powder of sample E3 using an Accupyc 1340 Helium Pycnometer.

A series of images were collected with the scanning electron microscope (SEM) at magnifications of 25× (three to five images for each thin section) and 100× (zero to three images for each thin section) (Appendix B). All images were processed in Adobe Photoshop to allow application of the FOAMS software to obtain the size and number of crystals (Shea et al., 2010). Larger crystals were acquired by scanning both the sectioned sample and the thin section with a desktop scanner in natural and polarized light following the procedure of Pioli et al. (2014). Finally, we used the CSDslice database (version 4, Morgan and Jerram, 2006) to determine the 3D crystal habit (long, intermediate and short axis), and the CSDCorrections 1.3 software (Higgins, 2000) to calculate the crystal size distribution (CSD) from FOAMS 2D data following the procedure from Thivet et al. (2020). This also allowed us to derive the percentage

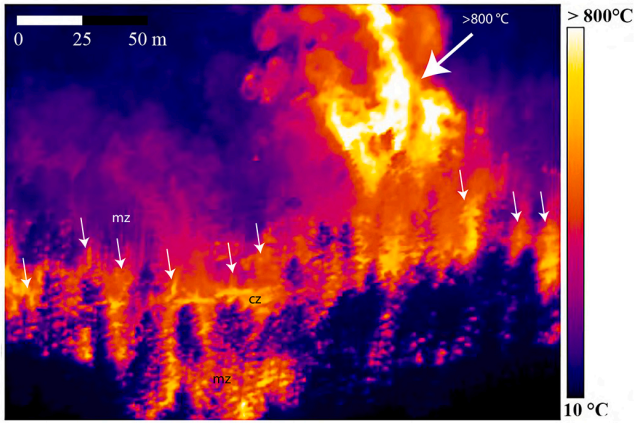

Fig. 4. Low-oblique helicopter-based image acquired 27 October 2002 at 14 h26 showing the Linguaglossa flow moving though forest. Following the model of Biren et al. (2020), we see all three stages of tree mold creation. Trees central to the flow (central zone, "cz") have been already felled and lost, their molds being over-run by the advancing lava stream. Trees proximal to the channel have already been heated and dried to the point where they have reached combustion (combustion zone, white arrows). Trees in the levees are surrounded by lava (marginal zone, "mz") but are not yet burning. These "mz" trees are, however, being heated and dried to the point where, eventually, they will combust, burn-through and become felled. Note, temperatures in the canopy that is in the process of combustion are (probably much) >800 °C (see Robinson (1991) for likely flame temperatures in this "fire canopy"). This zone is saturated in the thermal imagery and is indicated by the large white arrow labelled "> 800 °C".

Table 1
Sample details. Sample E03 is a near-vent bomb, all other samples are of the lava interior as sampled at levee and flow front (E10) ooze outs of glassy toothpaste lava (cf. Rowland and Walker, 1987) or of channel overflow of spiny pahoehoe (E04).

Sample label	GPS coordinates		Elevation (m asl)	Distance from vent (km)
	Latitude (N)	Longitude (E)		
E03	37°48′10.76″	15° 1′55.08″	1954	0.38
E04	37°48′6.73″	15° 2′8.77″	1882	0.74
E05	37°47′47.27″	15° 3′11.08″	1646	2.4
E06	37°47′53.10″	15° 3′37.38″	1555	3.08
E07	37°47′56.23″	15° 4′3.55″	1491	3.73
E08	37°47′57.24″	15° 4′3.31″	1490	3.73
E11	37°48′7.63″	15° 4′37.71″	1400	4.65
E01	37°48′11.32″	15° 4′53.09″	1356	5.05
E02	37°48′10.73″	15° 4′57.92″	1340	5.19
E09	37°48′22.56″	15° 5′55.35″	1126	6.65
E10	37°48′22.31″	15° 5′55.55″	1126	6.65

of phenocrystals and microphenocrysts in the lava (Table 5).

4. Results

We map Etna's 2002 Linguaglossa lava flow unit as being about 7 km long and occupying an area of 2.1 km^2. For the medial part, the flow is typically 200–250 m wide, but distally it is narrower (90–150 m) where it becomes contained in a ravine at the foot of the Piano della Pernicana fault scarp (Fig. 1). The flow field is a classic 'a'ā channel system (cf. Lipman and Banks, 1987), with a 6.7-km-long braided channel segment feeding a 0.3-km-long distal section of dispersed flow. Typically the rubble levees are around 9 m high and 10–30 m wide, and surround 20–50 m wide channels with flow level being 2–3 m below bank. In certain places, the levees are wider due to the presence of stalled lateral lobes and/or breakout flow from levee failure (e.g., Fig. 2).

The flow front itself is 50 m wide and comprises seven ooze-out lobes of inflated spiny (toothpaste) pāhoehoe (cf. Rowland and Walker, 1987). Each lobe is around 30 m long, 10–15 m wide, with well-formed inflation clefts running down their axes (cf. Walker, 1993). This is the unit that Andronico et al. (2009) describes as breaking out from the flow front after supply from the main vent had been cut. This late-stage breakout was caused "by channel emptying, and occurred when lava coming from the main vent was completely crusted over", and was active until 5 November (Andronico et al., 2009), i.e., for two days after supply from the vent had ceased. While only burnt and dead oaks were observed still standing at the flow front (although since felled by the Corpo Forestale, Fig. 5), charred but still living pines were ubiquitous within 5–15 m of the flow levees (Fig. 6).

4.1. Forest interaction

Comparison of imagery available on Google Earth (31/12/85 versus 15/09/2003 images) reveals that the main flow leaving the fissure immediately entered, and would have interacted with, the Linguaglosa pine forest along its entire length (Fig. 1). Indeed, felled trees lying on the flow surface, on the levees and on lava-free ground around the flow are apparent everywhere (Figs. 1 and 2). Felled trees are almost entirely black pines with straight trunks, which is consistent with this type of pine accounting for 95% of the Linguaglossa forest (Barreca et al., 2010) as well as our own measurements. At site E0, which characterized the forest across the proximal and medial sections of the flow, we counted 43 ± 3 trees across a 400 m^2 area to give a density of 0.11 ± 0.01 trees/m^2. This is identical to the tree density obtained by Barreca et al. (2010) for the Linguaglossa forest. All trees were black pines with heights of 20–25 m and trunk diameters of 20–80 cm. This compares with a mean height and diameter obtained by Barreca et al. (2010) of 27 m and 48 cm, respectively. Felled tree trunks have a median length of 8 m. Given the typical height of the pines in the Linguaglossa forest, this means that 70% of the trunk by length is typically consumed by combustion.

On the flow surface 4700 trees are apparent as trunks, being the remnants of trees that were felled by the flow to fall onto the flow surface. We use the tree density to estimate that around 231,000 trees covered the area now occupied by the flow unit before the eruption (Table 2). Thus, the 4700 felled trees mapped on the flow surface represent just 2% of the pre-eruption tree total. The remaining trees are not visible and, we infer, have been buried by the flow.

The flow orientation is between 45°N and 90°N. Felled tree orientation varies between 270°N and 90°N, with 41% of the orientations varying between 35°N and 100°N, meaning that they are sub-parallel to the flow direction (Fig. 7). This implies that trees were generally felled to topple onto the moving flow surface to then be carried by the flow for some distance, thus becoming aligned with the flow direction. The remaining 59% of the felled trees are, thus, not parallel to the flow direction. These trees are always those at the extreme edge of the flow, so that the trunk fell onto lava-free ground beside the flow so as not to be transported (Fig. 2). We note, also, that felled trees are only apparent at the channel margins (along the contact with the levees), and in the centre of the channel tree survival is zero (Fig. 1). This is with the exception of kīpukas or dagalas within the flow and at islands between channel branches in braided sections (Fig. 2). Fig. 3 also shows that the felled tree distribution down the flow is not homogenous. There are two zones relatively rich in felled trees, between 1.5 and 3.5 km and again between 4.5 and 6.5 km. In these two zones, trunk length of felled trees lying on the flow also tends to be longer, being 8–12 m (±1 m) in the first zone and 4–8 m (±1 m) in the second (Fig. 8a).

4.2. Channel type, tree interactions and flow velocities

The channel leaving the vent area (location "a" in Fig. 1), as imaged at 16:10 (hh:mm; all times are local, UTC + 1) on 2 November was 30–50 m wide, 2.5 ± 0.5 m deep and contained 'a'ā (Fig. 3a). By the time of the imagery of Fig. 3a, i.e., five days after flow onset, all trees had

Fig. 5. Partially burnt-through trunks surviving at the flow front. These trees remained standing, in spite of contact with the flow, but were later felled by the Corpo Forestale during security (controlled felling of dead trees) operations. Note, charring of the bark, and impact by ‘a‘ā clasts tumbling off of the flow front that was engulfing them at the time of flow front arrest. Trunks are 34 cm in diameter.

Fig. 6. Charring of tree trunk bark on sides facing the flow. Note that all trunks within 15 m of the flow are charred but still living, including some within 1 m of the flow, meaning that heating at this proximity was damaging but not fatal for the tree. Trunk is 80 cm across.

Table 2
Tree density, lava flow area, and tree counts from the Google Earth Image (Fig. 1). The flow area of 2.1 km^2 means that lava destroyed 18% of the 11.78 km^2 Linguaglossa pine forest. Error on the expected and missing trees is ±21,000.

Tree Density (trees/m^2)	0.11 ± 0.01
Lava flow area (m^2)	2.1 × 10^6
Expected trees (no.	231,000 (100%)
Digitalized trees (no.)	4700 (2%)
Missing trees (no.)	226,300 (98%)

been burnt and/or felled and buried so that the ‘a‘ā channel was well-established and tree-free by this point. Eighty-two thermal images were analysed to estimate the velocity at the central plug (43 images) and the marginal shear zones (39 images), giving a mean of 0.8 ± 0.1 m s^{-1} for the plug and 0.4 ± 0.2 m s^{-1} at the channel margins. This compares with a mean velocity calculated using Eq. (2) of 0.5 ± 0.2 m s^{-1} (Table 3) and yields an effusion rate of 60 ± 15 m^3 s^{-1}; comparable with peak values obtained from the satellite data by Harris et al. (2011, 2012), i.e., 20–60 m^3 s^{-1}. The agreement between measured and calculated ranges lends confidence to the result of applying Eq. (2) to derive velocities elsewhere.

The upper-medial channel (0.74 km from the vent, location “b” in Fig. 1), as imaged around 09:30 on 2 November was around 25 m wide, 2 ± 0.5 m deep and contained ‘a‘ā (Fig. 3b). As at the vent-leaving channel, by the time of the imagery of Fig. 3b, again five days after flow entry into the forest, all trees within the channel had been burnt and/or felled and buried. Broad (50 m wide) levees of stagnant, cooling lava were apparent, with trees still standing only at islands within the channel. Although within the channel and levees no standing trees are apparent, burning (but largely consumed) trees can be seen at the channel-levee margin (Fig. 3b). Flow velocities calculated using Eq. (2) were 0.4 ± 0.2 m s^{-1} (Table 3), giving an effusion rate of 50 ± 25 m^3 s^{-1}. This overlaps with the value estimated for the vent-leaving channel on the same day, meaning that our estimates are consistent in terms of down channel conservation of mass.

Between the upper-medial section and the flow front (location “c” in Fig. 1), the situation was similar. The image of Fig. 3c was acquired around 14:30 on 27 October (i.e., two days after flow onset) and again shows a well-established, tree-free ‘a‘ā channel between broad levees of cooling, stagnant ‘a‘ā flow. However, at this earlier time, trees are still standing in the levees, only some of which are burning. In addition, felled trunks, with their long axis aligned with the flow direction, can be seen floating on the channel surface (Fig. 3c). Channel velocities remain between 0.1 and 0.9 m s^{-1} for all stations, with flow thickness ranging between 5 and 11 m (Table 3). The flow front itself was around 9 m high, 50 m wide and moving, at the time of image capture in Fig. 3d, through a largely tree-free zone at the head of the “Vallone Salto del Bue” valley.

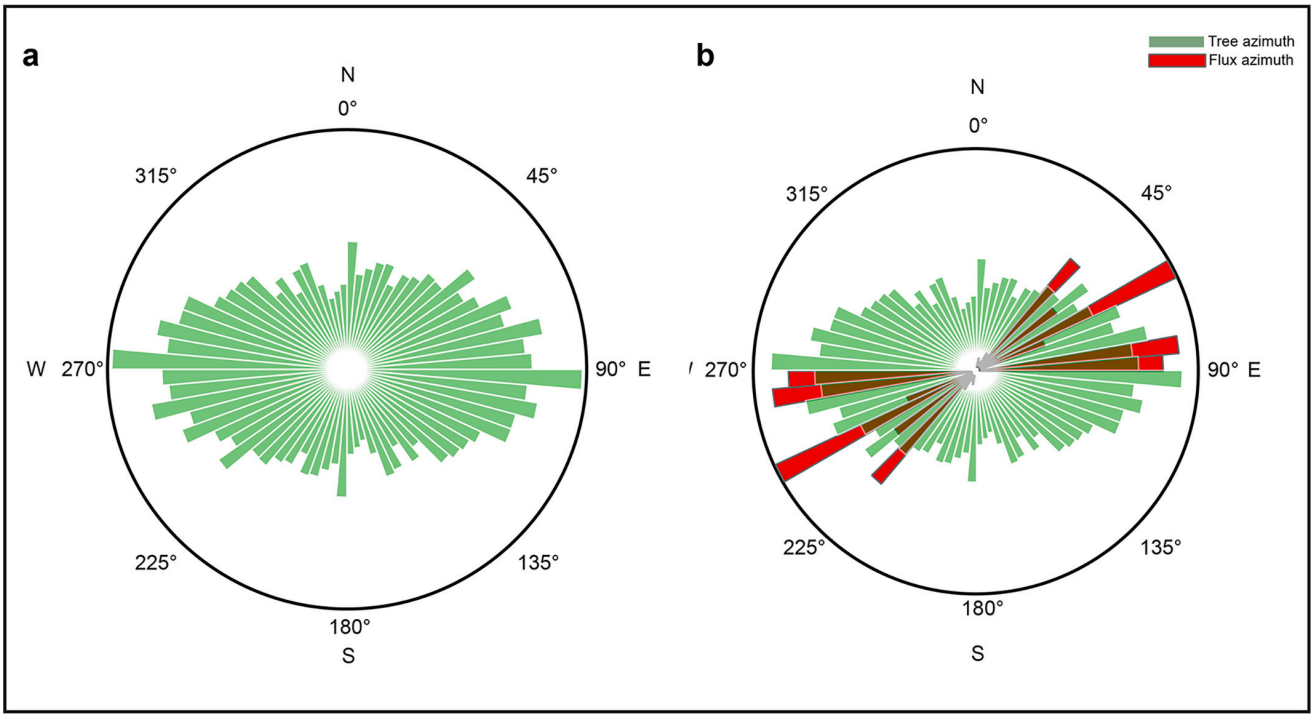

Fig. 7. Rose diagrams for tree azimuth without (a) and with (b) flow azimuth. Note two populations, a primary one orientated with flow azimuth (i.e., tree trunks aligned with the flow direction), and a secondary one at 45 ± 15° to the flow azimuth (i.e., trees falling away from the flow). (For interpretation of the references to colour in this figure legend, the reader is referred to the web version of this article.)

At this location, the flow itself is contained and channelized within a ravine of approximately the same width as the flow front and which follows the base of the Pernicana fault scarp (cf. Fig. 2 of Neri et al., 2005).

4.3. Down-flow surface temperatures, heat losses and cooling rates

Proximally, the flow surface temperature ranged between 350 °C and > 650 °C (Fig. 3a; Table 4), which translates to heat loss densities of 30–65 kW m^{-2} and cooling rates (typically) of 5.5 ± 0.3 °C km^{-1}. However, there is an isolated peak at 26.7 °C km^{-1} at 2.4 km (Fig. 8b) due to particularly low velocities at this location (Fig. 8a). After 3.1 km, surface temperatures are lower (380–445 °C), and heat loss densities are stable at 32 ± 4 kW m^{-2} (Table 4). Here, cooling rates per unit distance are a little more variable as they also depend on variations in velocity (Fig. 8b). High temperatures (>650 °C) are measured at the flow front (Fig. 3d) due to exposure of hot material by flow front extrusions of the flow interior and avalanching of material to expose hotter material deeper in the flow front breccia (cf. Harris et al., 2002). However, surface crust temperatures are generally lower than elsewhere, as apparent from the mean temperature of 320 °C, so that heat flux densities and cooling rates are lowest at the most distal locations (Table 4).

Around the channel we see hot spots that can be associated with burning trees (Fig. 3c), where flames result in temperatures of >650 °C. Temperatures in the flames associated with the burning tree canopy are at least 800 °C, the saturation point of the gain setting used. Thus, locally, the atmosphere overlying the flow was hotter than the active flow surface itself (cf. Table 4).

4.4. Chemical and textural analysis

Following the Total Alkali-Silica (TAS) classification, the composition of the ‘a‘ā flow is trachy-basaltic. Samples comprise plagioclase, clinopyroxene, olivine and oxides in a microcrystalline groundmass (Appendix B), thus exhibiting chemical and mineralogical associations typical of Etnean lavas (c.f. Andronico et al., 2005; Clocchiatti et al., 2004; Corsaro and Miraglia, 2005; Corsaro and Pompilio, 2004; Vona et al., 2011). We were able to group the crystals into three different populations by size: (i) phenocrysts with equivalent diameters between 1 and 8 mm; (ii) microphenocrysts with equivalent diameters between 0.2 and 1 mm; and (iii) microlites with equivalent diameters of <0.2 mm. Phenocryst and microphencryst size ranges for plagioclase and clinopyroxene are the same, being 1–8 mm and 0.5–1 mm, respectively. Microlites of plagioclase are smaller than those of clinopyroxene, being <0.1 mm as opposed to <0.5 mm.

We see no obvious down flow trend in crystal content (Fig. 9). Highest microlite crystallinities are for the at-vent sample and the flow front sample (Fig. 9). These samples are a bomb and flow front squeeze out of toothpaste lava, respectively (E3 and E10 Appendix B and Table 5). All other samples are ooze-outs of the channel core from the base of the levee. We therefore suggest that samples E03 and E10 underwent slower cooling than all other samples, which show relatively low microphencryst contents of 0.2–1.2 vol% (Table 5). If there was substantial down-flow cooling, we would expect an increase in the microphenocryst content with distance (cf. Cashman et al., 1999). Thus, we suggest that this low and moderately stable trend is indicative of well insulated (well-crusted) ‘a‘ā flow where cooling rates are minimized (cf. Table 4).

Phenocryst content also shows no down-flow trend, although there are two zones of relatively high values, between 0.7 and 3.1 km, and again around 5.1 km (Fig. 9). These zones correlate with relatively low flow velocities (cf. Fig. 8b). Because all of these samples were collected from the base of the levee, and therefore sampled the bottom of the flow, this could represent localized concentrations of phenocrysts due to crystal settling in low velocity zones (cf. Rowland and Walker, 1987). We favour this mechanism to explain these peaks because phenocryst contents in these zones are greater than that of the at-vent control sample (i.e., 31% for the bomb, E03, Table 5). The E03 phenocryst

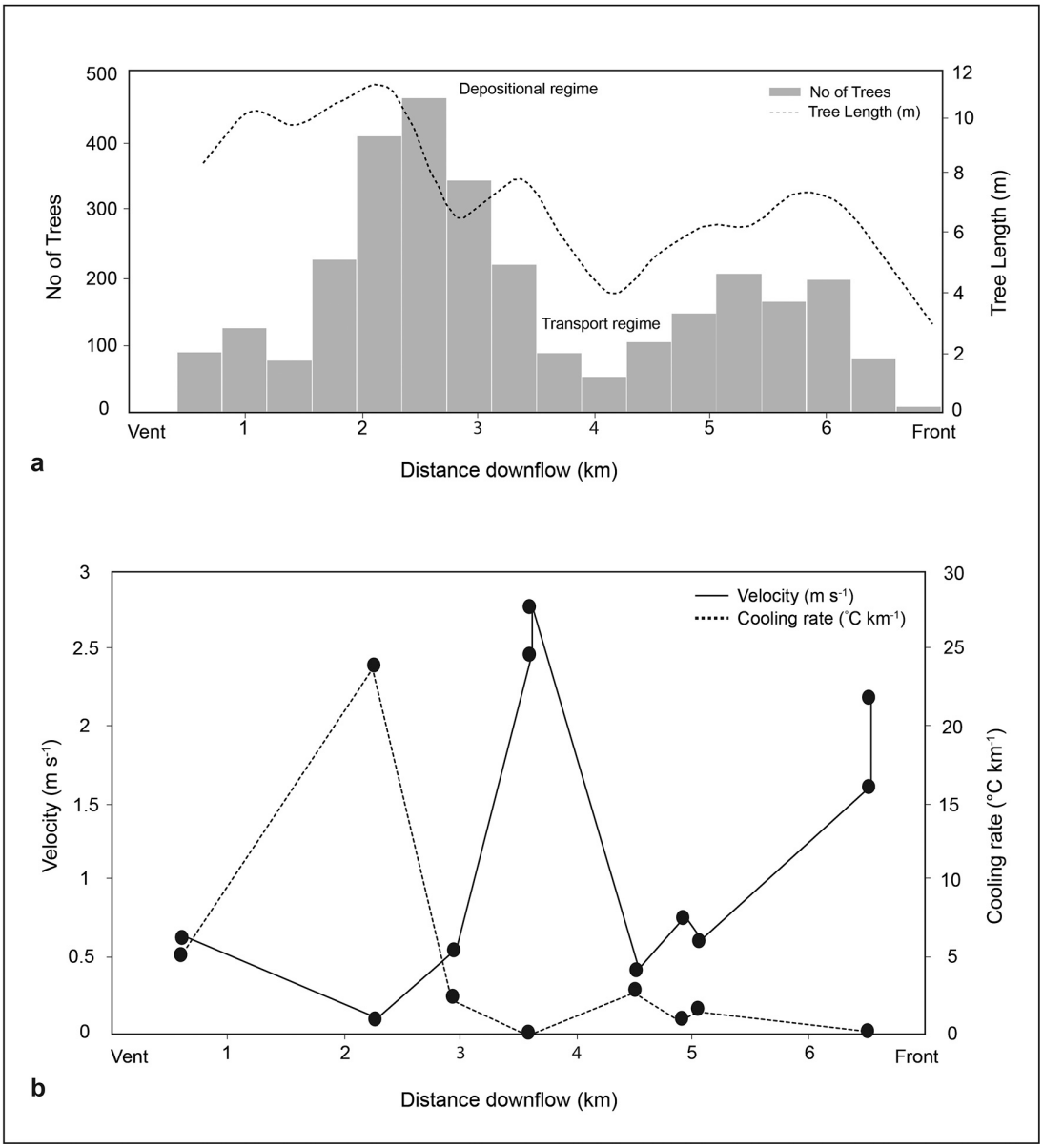

Fig. 8. Tree trunk distributions with distance from the vent as apparent from the imagery of Fig. 1 and flow dynamics. (a) Variation in number of trees and tree lengths with distance down-flow, note zones of deposition and transport, i.e., zones with a high and low number of tree trunks apparent on the flow surface, respectively. The histogram bins start from 500 m because there are no trees before this point. (b) Down-flow variation in velocity and cooling rates showing high and low velocities in the zones of transport and deposition, respectively.

content is also more typical of Etnean lavas, which are porphyritic with phenocryst contents of 30–40% (e.g., Armienti et al., 1994; Tanguy et al., 1973). We therefore suggest that down-flow values increasing to >50% are the result of local concentrations at the flow base due to crystal settling in low energy environments.

Density varies between 1320 and 2610 kg m^{-3} with an average of 1940 ± 400 kg m^{-3}. The DRE is 2870 kg m^{-3}, so the bulk values convert to vesicularities of 9 to 54%, with an average of 32 ± 14% (Table 5). Highest vesicularities of around 50% are found for the at- and near-vent samples, with lower values (around 10–40%) thereafter, but with no systematic down flow trend (Table 5 and Appendix B). Samples are characterized by mm- to cm-sized vesicles which are extensively interconnected, with irregular shapes (Appendix B), which is typical for ‘a‘ā lava.

5. Discussion

The Linguaglossa lava flow destroyed and buried the Piano Provenzana tourist infrastructure (Andronico et al., 2005), plus 2.1 km^2 of forest through which it moved, causing fires (Fig. 6). Around 231,000 trees covered the area before the eruption (Table 2), of which none remained standing following passage of the flow, and just 2% were still apparent as trunks lying on the flow surface. Tree molds were also exceedingly rare. Across the 0.15 km^2 area covered by the UAV overflight of Fig. 2, we found two tree molds. The rare tree molds were only found at the base of the lateral levees (e.g., Fig. 10). Extrapolating this density (13 molds per km^2) to the entire flow area gives a total expected tree mold count of just 28. No lava trees were found at any of our sample sites. However, Carveni et al. (2011) do report a lava tree at the flow margin in the proximal region (at the Piano Provenzana). The

Table 3
Slope, thickness of lava in channel and density measured for sample site, and derived velocity (Eq. (2)). Regime is in terms of whether trees are transported (T) or deposited (D), and "NA" means that the calculation and regime is not applicable as the sample is a bomb, not lava (see Table 1).

Sample label	Distance from vent (km)	Slope (°)	Lava thickness (m)	Lava bulk density (kg m^{-3})	Flow velocity (m s^{-1})	Regime
E03	0.38	11.5	NA	1460	NA	NA
E04	0.74	11.5	2.5	1320	0.5	T
E05	2.4	7.4	2	2090	0.4	D
E06	3.08	7.4	5	1755	0.2	D
E07	3.73	5.2	11	2320	0.8	T
E08	3.73	5.2	11	2615	0.9	T
E11	4.65	5.7	5	1765	0.1	D
E01	5.05	6.3	6	1995	0.3	D
E02	5.19	6.3	5	2305	0.2	D
E09	6.65	7.4	9	1570	0.5	T
E10	6.65	7.4	9	2135	0.7	T

Table 4
Flow surface temperatures and derived heat flux density (Eq. (3)) and cooling rate (Eq. (6)).

Sample label	Distance from vent (km)	Temperature (°C)				Heat flux density (kW m^{-2})	Cooling Rate (°C km^{-1})
		Max	Min	Mean	St Dev.		
E04	0.74	650	350	610	42	65	5.5
E05	2.4	535	350	410	36	32	25.7
E06	3.08	650	360	440	60	36	2.6
E07	3.73	460	365	405	22	31	0.2
E08	3.73	460	365	405	22	31	0.1
E11	4.65	495	390	425	30	33	3.1
E01	5.05	430	350	385	21	28	1.1
E02	5.19	530	375	445	42	36	1.8
E09	6.65	650	320	385	59	29	0.5
E10	6.65	650	320	385	59	29	0.2

interaction was thus largely destructive, and from the proximal-medial reach onwards there was no preservation of trees or lava trees. The main evidence of forest interaction is the ubiquitous presence of charred trunks of felled trees lying on the surface of the flow, but which are apparent only at the channel margins and levees (Fig. 2). We here discuss the mechanics of this destructive interaction and the thermal effects of tree burning on the flow, before considering mold formation in ʻaʻā and the resultant structures.

5.1. Mechanical interaction

There were two types of mechanical interaction between the flow and the forest: entirely destructive and partially destructive. These interactions were located at the flow centre and margins, respectively. Across the central portion of the flow front, where later the channel became established, the interaction was entirely destructive. Examination of trees at the flow front shows that the mechanical force of the advancing flow pushing the tree into an unstable position, the tree then falling in the flow direction and splintering, with Fig. 11 showing that the onset of splintering could occur before felling. Note that the still-standing tree of Fig. 5 is also beginning to splinter, indicating that splintering likely the proceeds the felling event. Trunk orientation for trees at the fronts of stalled lateral lobes and levee breakouts are all, thus, in the flow direction (Fig. 2). The absence of felled trunks on the surface of the channel (cf. Figs. 1 and 2) leads us to suggest that, once felled onto the ground in front of the flow, the trunk was buried by the advancing flow front to become part of the basal crust. This was the fate of 80% of the forest, i.e., the unaccounted tree population of 20,600 in Table 2.

The environment at the flow margins was less destructive. Here, trees generally became incorporated in the channel levees. Field evidence shows that trees became buried at their bases by clasts avalanching down the levee margin. The buried portion of the trunk then slowly burnt through, so that the exposed portion of the trunk became felled (Fig. 10). A few trees did not entirely burn through and remained standing at the flow edges (Fig. 3). Trees at the edge of the levee were all buried by hot ʻaʻā clasts avalanching down the levee sides, rather than being engulfed in fluid lava as is the case for molds in Hawaii (cf. Finch, 1931; Lockwood and Williams, 1978), as tree molds expose only breccia (Fig. 12). These trees tended to fall away from the flow and onto the surface of the levee or lava-free ground beside the levee (Fig. 2), orientating themselves at an angle away from that of the flow direction (Fig. 7). This was helped by blocks rolling down the levee side to cause a final felling event that was in a direction tangential to that of the flow direction, but the same as the rock fall direction (Fig. 13). Indeed, many trunks have charred (black) bases and a degree of shattering and snapping (Fig. 13), indicating that they were weakened by burning and then broken by clast impact. This population of trunks contributed to the levees, so that the levees became a mixture of rubble and felled trees (Fig. 13).

Trees falling onto the moving channel appear to have become orientated in the down-flow direction, and concentrated at the channel edge to become clustered at the levee contact (Fig. 1). This likely resulted from a parabolic cross-channel velocity profile that rotated the trees into the down-flow direction and pushed them towards the channel

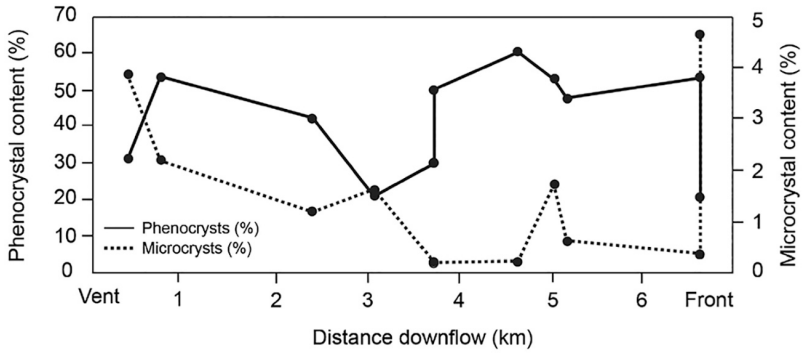

Fig. 9. Down-flow variation in microphenocrysts and phenocrysts. Note two zones of phenocryst concentration which related to lower velocity reaches where crystal contents are enhanced by settling. The highest values for microphenocrysts are for the at-vent (bomb) and flow front (frontal toothpaste flow) samples, all other samples are ooze outs at the levee base and have similar (low) values.

Table 5
Summary of sample textural data.

Sample label	Distance from vent (km)	Bulk density (kg m^{-3})	Vesicularity (%)	Total phenocryst content (%)	Total microphenocryst content (%)
E03	0.38	1460	49	31	3.9
E04	0.74	1320	54	54	2.2
E05	2.4	2090	27	42	1.2
E06	3.08	1755	39	21	1.6
E07	3.73	2320	19	30	0.2
E08	3.73	2615	9	50	0.2
E11	4.65	1765	39	60	0.2
E01	5.05	1995	31	53	1.7
E02	5.19	2305	20	48	0.6
E09	6.65	1570	45	54	0.4
E10	6.65	2135	26	21	4.7

Fig. 10. Tree mold in the base of the left-bank rubble levee with tree responsible for the mold felled to the right. Note that the lower portion of the trunk has burnt through, but the upper portion survives. Tree mold is around 75 cm across, and is at location marked "x" in Fig. 2.

margin. We note also that down flow concentrations of trunk incidence coincide with zones of lower calculated channel velocity (Fig. 8), where there are two zones of trunk transport where velocities are between 0.5 and 1 m s^{-1}, and two zones of deposition where velocities are <0.5 m s^{-1}. Thus, whether tree trunks were deposited to contribute to the levee depended on the velocity of the system. The same zones of deposition and conditions for concentration appear to also apply to crystal settling (Fig. 9).

5.2. *Thermal interaction*

We were unable to collect glass samples to check down-flow cooling, but cooling rates derived from the heat fluxes were 0.1–5.5 °C km^{-1}. This is comparable with cooling rates measured for tree-free cases that typically range between 4 and 9 °C km^{-1} (Cashman et al., 1999; Chevrel et al., 2019; Crisp et al., 1994; Rhéty et al., 2017; Riker et al., 2009; Robert et al., 2014; Soule et al., 2004). Normal cooling rates are also consistent with the results of Chevrel et al. (2019), who found no abnormalities in cooling rates down a channel containing lava trees on Kīlauea, where cooling rates were 4–10 °C km^{-1}. Thus, we believe there to have been no measurable thermal interaction, and thus no enhanced or diminished cooling due to the presence of the trees. If anything, the cooling rates are slightly lower than other channelized cases from Kīlauea, Mauna Loa and Piton de La Fournaise (e.g., Cashman et al., 1999; Rhéty et al., 2017; Riker et al., 2009), a result of the thermal insulation provided by the thick, stable, cool surface breccia on this ʻaʻā flow (cf. Fig. 3d).

Likewise, crystal content, vesicularity and chemistry are normal for Etnean ʻaʻā lava flows (Table 5), so that interaction with the forest had no textural effect on the flow either. In fact, the lack of increase in crystallization down channel shows that the flow was particularly well insulated. This is also as we would expect from a well-crusted ʻaʻā flow where, as stated above, the thick brecciated crust provides extremely effective insulation to minimize cooling and crystallization rates (cf. Harris et al., 2002). Again, this is consistent with no abnormalities in the down flow cooling rate. It is also consistent with the detailed analysis of a tree mold by Biren et al. (2020), who found that interactions (chemical, thermal, and textural) were limited to the quenched lava at the tree-lava contact, with no effects after a distance of a few millimetres. As a result, the presence of the trees plays no role in changing the thermal or textural bulk properties of the flow away from normal (tree-free) conditions.

Temperatures in fires burning in the canopy above the flow (e.g., Fig. 4) were higher than the flow surface itself. This means that the term

Fig. 11. Mode of tree destruction for trees in the path of the ʻaʻā flow. The tree was in the process of being felled when forward motion of a lateral lobe stopped. Flow direction is left-to-right. Tree is being pushed in the same direction, and beginning to splinter on the up-flow side. Trunk is ~1.5 m high.

Fig. 12. Magnifications of tree mold of Fig. 10. Note that the walls are of ʻaʻā breccia, not of solid lava of the flow interior as found quenched around trees molds in pāhoehoe (Lockwood and Williams, 1978; Lockwood and Hazlett, 2010). Pre-existing surface with charred vegetation remains are apparent at the base of the mold. This defines the form of a tree mold as forming in ʻaʻā. Tree mold is around 75 cm across, and is at location marked "x" in Fig. 2.

Fig. 13. Mode of tree destruction for trees in the levees of the ʻaʻā flow. Note: blocks lying against or on the tree trunks, and shattered and charred bases. (a) Unfelled tree with block that has tumbled down the levee resting against the trunk, tree in background (black arrow) is being pushed laterally away from the flow. Tree trunk is about 75 cm across. (b) Two-meter block ("B") lying on felled trunk, block impact has snapped and shattered the trunk. (c) One-meter block ("B") lying on felled trunk, tree trunk base is charred where the tree was largely burnt through at the base at the time of felling, and its mold buried by the rock fall event. (d) Shattered tree trunks felled laterally by rock falls off the levee with molds buried by the rock fall events. For scale, tree trunks are around 50 cm across.

T_s^4-T_a^4 in Eq. (4) will be negative and heat will flow from the fire to the surface under such conditions. This will have a further insulating effect. However, these effects will be temporally and spatially limited. For example, in Fig. 3 we see that there are no burning trees above the main channel five days after the eruption onset, so that this effect would just have applied to lava flow emplacement in the first few days. Instead, in Fig. 4 we see that the fire canopy is just 50 m wide. A flow moving at 0.5–0.9 m s^{-1} will be through the fire canopy zone in 1–2 min. Thus, the time of exposure to these abnormal atmospheric conditions will also be of limited duration even when it does apply, with normal conditions operating thereafter.

5.3. *ʻAʻā tree mold formation*

We can here define the form of tree molds forming in ʻaʻā flows and their mechanism of formation. They form by being slowly surrounded by hot breccia tumbling down the levee sides (Fig. 13). In the same manner as formation of tree molds in pāhoehoe, the buried part of the trunk slowly heats, dries and eventually combusts (cf. Biren et al., 2020) to burn away so that, eventually, the exposed part of the tree is felled, leaving a cast of its combusted trunk in the engulfing lava (cf. Lockwood and Hazlett, 2010). We see from Fig. 3 that trees are still standing in the levees after three days but not after five days, so that the time scale of combustion in this case is several days. This compares with around 12 h (for the time needed to heat, dry and combust the tree) for a tree surrounded by pahoheoe on Kīlauea as analysed by Biren et al. (2020). This difference is likely due to the differences in water content of the trees and wood density between the two cases, as well as the thermal character of the two surfaces of the two lava flow types (pāhoehoe and ʻaʻā).

Because the vertical molds considered here form in the levee breccia, tree molds have irregular, rough walls of ʻaʻā clasts (e.g., Figs. 10 and 12), rather than smooth walls of solid, quenched lava that is the case in pāhoehoe (cf. Finch, 1931; Lockwood and Williams, 1978). As in tree molds forming in pāhoehoe, though, the pre-existing surface (cf. Parcheta et al., 2012; Jones et al., 2017) and carbonized plant material (cf. Moore and Richter, 1962) can be seen on their floors (Fig. 12). However, vertical molds are rare in the ʻaʻā flow type case as they tend to be filled and buried by subsequent breccia avalanching down the levee sides (Fig. 13).

Carveni et al. (2011) noted a similar form to horizontal molds

forming in the basal breccia of a prehistoric flow on Etna's south flank, where the walls were "rough due to the presence of 'a'ā clasts in the walls". Carveni et al. (2011) also suggested that they resulted from trees "rolled along in the basal clinker layer". Thus, horizontal mold formation in 'a'ā involves those trees felled by flow advance so that the tree falls into the path of the advancing flow to be incorporated into the basal breccia. Here, they slowly burn away, or rot away if in an anoxic environment (Bella and Gaál, 2007), to leave horizontal molds or "caves" of the same dimensions of the combusted trunk. For our case, this was the fate of 80% of the trees (20,600, or around one tree every 10 m^2), so in basal breccias of 'a'ā flows that have moved through densely forested areas horizontal tree molds should be common.

6. Conclusion

'a'ā flows are generally viewed as destructive in terms of lava tree and tree mold preservation, the mechanical interaction being one whereby the advancing flow fells all trees in its path. Although we see no thermal interaction (i.e., no enhanced or dampened cooling or crystallization of the flow) due to consumption of these felled trees or fire canopy effects (cf. Fig. 4), we do see a mechanical interaction.

The mechanical interaction varies between the flow central axis (the channel) and the flow margins (levee). Trees central to the flow axis of advance (98% of the trees considered here) are pushed over, with their trunks being snapped and splintered, in a direction parallel to flow direction to then be overrun by the flow. On the other hand, trees on the levee outer flank are slowly consumed by hot rubble avalanching from the levees, to then be knocked over by the same avalanches to orientate themselves at right angles to the flow direction. Thus, these trees tend to be felled not by burn-through, as is the case traditionally (cf. Finch, 1931; Lockwood and Hazlett, 2010; Biren et al., 2020), but by knock-over. Instead, buried sections of trees at the channel-levee contact are in a much hotter environment and eventually burn through and felled so that the exposed section of the trunk is transported at the edge of the channel, the felled trunks becoming orientated with flow direction and deposited where velocities are lowest. This population of felled-trees thus becomes part of the levee construct, which becomes a mixture of organic and inorganic material. The latter will, in time, decompose and will not be apparent in the geological record. Trees rolled beneath the flow will also rot, or burn, away to leave horizontal tree molds in the basal breccia. These, however, will be apparent in the geological record as horizontal "caves", as will vertical tree molds formed by trunk burial in rubble levees.

Thus, in agreement with Carveni et al. (2011), we find that 'a'ā flows do interact with trees. The resulting tree molds, and surviving trunks, thus provide information on flow emplacement conditions, as in the case of pāhoehoe flows (e.g., Lockwood and Williams, 1978; Parcheta et al., 2012; Jones et al., 2017; Chevrel et al., 2019). While trunk orientation gives information on flow directions, area density gives information on flow velocity and kinetic energy, and association (levee versus channel) allows formation environment to be ascertained (cool levee edge, versus hot channel margin). We thus highlight the fact that consideration and analysis of lava flow advance on a vegetated volcano should not ignore the key element of the emplacement environment, i.e., the trees.

Author contribution

AH completed all fieldwork, mapping and sampling in February 2017, oversaw the work, was responsible for the final write up, and managed the ANR-LAVA project and concept on which this work is based and from which this work was supported. SC collected all thermal images during the 2002 events, and NV collected and processed all drone and pole based data. SM, under the guidance of MF, mapped all trees and produced all tree statistic information, and was responsible for drafting Figures based on these data. SM, under the guidance of SC, also carried out all analyses of the thermal imagery. LC performed all textural and petrological analyses under the guidance of LG. OC aided with field work, and refinement of concepts. All authors contributed to writing the manuscript.

Data availability

All textural and chemical data are freely available via the DynVolc (http://wwwobs.univ-bpclermont.fr/SO/televolc/dynvolc/) observation system and database managed by LG. All other data are available subject to request. Thermal imagery are the property of INGV-OE, drone and pole data are of NV, and tree-orientation are of SM. All photos are from AH.

Declaration of Competing Interest

All authors have contributed to, seen and approved the final version of the manuscript being submitted.

Acknowledgements

This research was financed by the Agence National de la Recherche through the project LAVA (Program: DS0902 2016; Project: ANR-16 CE39-0009). We very much thank Sean I. Peters and an anonymous reviewer for their extremely constructive advice and support. This is ANR-LAVA contribution no. 23 and Laboratory of Excellence ClerVolc contribution no. 552.

Appendix A. Supplementary data

Supplementary data to this article can be found online at https://doi.org/10.1016/j.jvolgeores.2022.107621.

References

Andronico, D., Branca, S., Calvari, S., Burton, M., Caltabiano, T., Corsaro, R.A., Del Carlo, P., Garfì, G., Lodato, L., Miraglia, L., Murè, F., Neri, M., Pecora, E., Pompilio, M., Salerno, G., Spampinato, L., 2005. A multi-disciplinary study of the 2002–03 Etna eruption: insights into a complex plumbing system. Bull. Volcanol. 67 (4), 314–330. https://doi.org/10.1007/s00445-004-0372-8.

Andronico, D., Cristaldi, A., Del Carlo, P., Taddeucci, J., 2009. Shifting styles of basaltic explosive activity during the 2002-03 eruption of Mt. Etna, Italy. J. Volcanol. Geotherm. Res. 180 (2–4), 110–122. https://doi.org/10.1016/j.jvolgeores.2008.07.026.

Armienti, P., Pareschi, M.T., Innocenti, F., Pompilio, M., 1994. Effects of magma storage and ascent on the kinetics of crystal growth. Contrib. Mineral. Petrol. 115 (4), 402–414. https://doi.org/10.1007/BF00320974.

Barreca, L., Coletta, V., Gentile, F., Marziliano, P.A., Scuderi, A., 2009. Struttura delle pinete di laricio dell'Etna: il caso della pineta Ragabo. In: Ciancio, O. (Ed.), Atti del Terzo Congresso Nazionale di Selvicoltura per il Miglioramento e la conservazione dei boschi italiani. Accademia Italiana di Scienze Forestali I, pp. 95–100. https://doi.org/10.4129/CNS2008.011. Taormina (ME) 16-19 ottobre 2008.

Barreca, L., Marziliano, P.A., Menguzzato, G., Scuderi, A., 2010. Avifauna e struttura nella pineta Ragabo (Linguaglossa, CT). Forest@ 7, 223–233. http://www.sisef.it/forest@/.

Bella, P., Gaál, L., 2007. Tree mould caves within the framework of cave genetic classification. Nat. Conserv. 63, 7–11.

Bertile, W., 1987. *Des coulées volcaniques à Saint-Philippe (Mars 1986): gestion d'une catastrophe naturelle* (Edition Co).

Biren, J., Harris, A., Tuffen, H., Chevrel, M.O., Gurioli, L., Vlastélic, I., Schiavi, F., Benbakkar, M., Fonquernie, C., Calabro, L., 2020. Chemical, textural and thermal analyses of local interactions between lava flow and a tree – Case study From Pāhoa, Hawai'i. Front. Earth Sci. 8, 233. https://doi.org/10.3389/feart.2020.00233.

Calvari, S., Cotteli, M., Neri, M., Pompilio, M., Scribano, V., 1994. The 1991-1993 Etna eruption: chornology and lava flow-field evolution. Acta Vulcanol. 4, 1–14.

Carveni, P., Mele, G., Benfatto, S., Imposa, S., Puntillo, M.S., 2011. Lava trees and tree molds ("cannon stones") of Mt. Etna, 633–638. https://doi.org/10.1007/s00445-011-0446-3.

Cashman, K.V., Thornber, C., Kauahikaua, J.P., 1999. Cooling and crystallization of lava in open channels, and the transition of pāhoehoe lava to 'a'ā. Bull. Volcanol. 61, 306–323. https://doi.org/10.1007/s004450050299.

Chevrel, M.O., Harris, A.J.L., Ajas, A., Biren, J., Gurioli, L., Calabrò, L., 2019. Investigating physical and thermal interactions between lava and trees: the case of Kīlauea's July 1974 flow. Bull. Volcanol. 81 (2), 1–6. https://doi.org/10.1007/s00445-018-1263-8.

Clocchiatti, R., Condomines, M., Guénot, N., Tanguy, J.-C., 2004. Magma changes at Mount Etna: the 2001 and 2002–2003 eruptions. Earth Planet. Sci. Lett. 226 (3), 397–414. https://doi.org/10.1016/j.epsl.2004.07.039.
Corsaro, R.A., Miraglia, L., 2005. Dynamics of 2004–2005 Mt. Etna effusive eruption as inferred from petrologic monitoring. Geophys. Res. Lett. 32 (13) https://doi.org/10.1029/2005GL022347.
Corsaro, R.A., Pompilio, M., 2004. Dynamics of Magmas at Mount Etna. In: Mt. Etna: Volcano Laboratory, pp. 91–110. https://doi.org/10.1029/143GM07.
Crisp, J., Cashman, K.V., Bonini, J.A., Hougen, S.B., Pieri, D.C., 1994. Crystallization history of the 1984 Mauna Loa lava flow. J. Geophys. Res. 99 (B4), 7177–7198. https://doi.org/10.1029/93JB02973.
Favalli, M., Fornaciai, A., Pareschi, M.T., 2009. LIDAR strip adjustment: application to volcanic areas. Geomorphology 111 (3–4), 123–135. https://doi.org/10.1016/j.geomorph.2009.04.010.
Favalli, M., Fornaciai, A., Nannipieri, L., Harris, A., Calvari, S., Lormand, C., 2018. UAV-based remote sensing surveys of lava flow fields: a case study from Etna's 1974 channel-fed lava flows. Bull. Volcanol. 80 (3), 29. https://doi.org/10.1007/s00445-018-1192-6.
Finch, R.H., 1931. Lava tree casts and tree molds [abs.]. Geol. Soc. Am. Bull. 42, 299.
Gauthier, F., 1973. Field and laboratory studies of the rheology of Mount Etna lava. Philos. Trans. Royal Soc. London A: Math. Phys. Eng. Sci. 274 (1238), 83–98.
Harris, A., 2013. Thermal Remote Sensing of Active Volcanoes: A User's Manual. Cambridge University Press. https://doi.org/10.1017/CBO9781139029346.
Harris, A.J.L., Allen, J.S., 2008. One-, two- and three-phase viscosity treatments for basaltic lava flows. J. Geophys. Res. 113, B09212. https://doi.org/10.1029/2007JB005035.
Harris, A.J.L., Flynn, L.P., Matías, O., Rose, W.I., 2002. The thermal stealth flows of Santiaguito dome, Guatemala: Implications for the cooling and emplacement of dacitic block-lava flows. Bull. Geol. Soc. Am. 114 (5), 533–546. https://doi.org/10.1130/0016-7606(2002)114<0533:TTSFOS>2.0.CO;2.
Harris, Andrew J.L., Dehn, J., Calvari, S., 2007. Lava effusion rate definition and measurement: a review. Bull. Volcanol. 70 (1), 1–22. https://doi.org/10.1007/s00445-007-0120-y.
Harris, A., Steffke, A., Calvari, S., Spampinato, L., 2011. Thirty years of satellite-derived lava discharge rates at Etna: Implications for steady volumetric output. J. Geophys. Res. Solid Earth 116 (8), 1–15. https://doi.org/10.1029/2011JB008237.
Harris, A., Steffke, A., Calvari, S., Spampinato, L., 2012. Erratum: thirty years of satellite-derived lava discharge rates at Etna: implications for steady volumetric output (Journal of Geophysical Research B: Solid Earth 116 (B08204) DOI: 10.1029/2011JB008237). J. Geophys. Res. Solid Earth 117 (8), 5–6. https://doi.org/10.1029/2012JB009431.
Higgins, M.D., 2000. Measurement of crystal size distributions. Am. Mineral. 85, 1105–1116.
Houghton, B.F., Wilson, C.J.N., 1989. A vesicularity index for pyroclastic deposits. Bull. Volcanol. 51 (6), 451–462. https://doi.org/10.1007/BF01078811.
Jeffreys, H., 1925. The flow of water in an inclined channel of rectangular section. Philos. Magasin, serie 6 (4), 293,793–807.
Jones, T.J., Llewellin, E.W., Houghton, B.F., Brown, R.J., 2017. Proximal Lava Drainage Controls on Basaltic Fissure Eruption Dynamics, pp. 1–15.
Keszthelyi, L., 1995. Measurements of the cooling at the base of pāhoehoe flows. Geophys. Res. Lett. 22, 2195–2198.
Kilburn, C.R.J., Guest, J.E., 1993. 'A'ā lavas of Mount Etna, Sicily. In: Active Lava. UCL Press, London, pp. 73–106.
Lipman, P.W., Banks, N.G., 1987. Aa flow dynamics, Mauna Loa 1984. US Geol. Surv. Prof. Pap. 1350, 1527–1567.
Lockwood, J.P., Hazlett, R.W., 2010. Volcanoes Global Perspectives. Wiley-Blackwell.
Lockwood, J.P., Williams, I.S., 1978. Lava trees and tree moulds as indicators of lava flow direction, 115 (November 1975), 69–74.
Lockwood, J.P., Tilling, R.I., Holcomb, R.T., Klein, F., Okamura, A.T., Peterson, D.W., 1999. Magma Migration and Resupply during the 1974 Summit Eruptions of Kīlauea Volcano, Hawai'i. In: U.S. Geological Survey Professional Paper, 1613, p. 37.
Lormand, C., Harris, A.J.L., Chevrel, M.O., Calvari, S., Gurioli, L., Favalli, M., Fornaciai, A., Nannipieri, L., 2020. The 1974 west flank eruption of Mount Etna: a data-driven model for a low elevation effusive event. Front. Earth Sci. xx https://doi.org/10.3389/feart.2020.590411.
Macdonald, G.A., Abbott, A.T., Peterson, F.L., 1983. Volcanoes and the Sea. University of Hawaii Press.
Marchese, E.P., 1991. Piante e fiori dell'Etna. Sellerio, Palermo, p. 198.
Moore, H.J., Kachadoorian, R., 1980. Estimates of lava-flow velocities using lava trees. Rep. Plan. Geol. Prog. 1979–1980, 201–203.
Moore, J.G., Richter, D.H., 1962. Lava tree molds of the september 1961 eruption, Kīlauea volcano, Hawaii. Geol. Soc. Am. Bull. 73, 1153–1158.
Morgan, D.J., Jerram, D.A., 2006. On estimating crystal shape for crystal size distribution analysis. J. Volcanol. Geotherm. Res. 154 (1–2), 1–7. https://doi.org/10.1016/j.jvolgeores.2005.09.016.
Neri, M., Acocella, V., Behncke, B., Maiolino, V., Ursino, A., Velardita, R., 2005. Contrasting triggering mechanisms of the 2001 and 2002-2003 eruptions of Mount Etna (Italy). J. Volcanol. Geotherm. Res. 144 (1-4 SPEC. ISS), 235–255. https://doi.org/10.1016/j.jvolgeores.2004.11.025.
Parcheta, C.E., Houghton, B.F., Swanson, D.A., 2012. Hawaiian fissure fountains 1: Decoding deposits-episode 1 of the 1969-1974 Mauna Ulu eruption. Bull. Volcanol. 74 (7), 1729–1743. https://doi.org/10.1007/s00445-012-0621-1.
Pinkerton, H., Sparks, R.S.J., 1978. Field measurements of the rheology of lava. Nature 276, 383–385.
Pioli, L., Pistolesi, M., Rosi, M., 2014. Transient explosions at open-vent volcanoes: the case of Stromboli (Italy). Geology 42 (10), 863–866. https://doi.org/10.1130/G35844.1.
Rhéty, M., Harris, A.J.L., Villeneuve, N., Gurioli, L., Médard, E., Chevrel, M.O., Bachèlery, P., 2017. A comparison of cooling-limited and volume-limited flow systems: Examples from channels in the Piton de la Fournaise April 2007 lava-flow field. Geochem. Geophys. Geosyst. 18 (9), 3270–3291. https://doi.org/10.1002/2017GC006839.
Riker, J.M., Cashman, K.V., Kauahikaua, J.P., Montierth, C.M., 2009. The length of channelised lava flows: insight from the 1859 eruption of Mauna Loa Volcano, Hawaii. J. Volcanol. Geotherm. Res. 183, 139–156.
Robert, B., Harris, A., Gurioli, G., Medard, E., Sehlke, A., Whittington, A., 2014. Textural and rheological evolution of basalt flowing down a lava channel. Bull. Volcanol. 76, 824.
Robinson, J.M., 1991. Fire from space: global fire evaluation using infrared remote sensing. Int. J. Remote Sens. 12, 3–24. https://doi.org/10.1080/01431169108929628.
Rowland, S.K., Walker, G.P.L., 1987. Toothpaste lava: Characteristics and origin of a lava structural type transitional between pāhoehoe and aa. Bull. Volcanol. 49 (4), 631–641. https://doi.org/10.1007/BF01079968.
Shea, T., Houghton, B.F., Gurioli, L., Cashman, K.V., Hammer, J.E., Hobden, B.J., 2010. Textural studies of vesicles in volcanic rocks: an integrated methodology. J. Volcanol. Geotherm. Res. 190 (3–4), 271–289. https://doi.org/10.1016/j.jvolgeores.2009.12.003.
Soule, S.A., Cashman, K.V., Kauahikaua, J.P., 2004. Examining flow emplacement through the surface morphology of three rapidly emplaced, solidified lava flows, Kīlauea Volcano, Hawai'i. Bull. Volcanol. 66 (1), 1–14. https://doi.org/10.1007/s00445-003-0291-0.
Tanguy, J., Tazieff, H., Cristofolini, R., 1973. The 1971 etna eruption: petrography of the lavas. Philos. Trans. Royal Soc. London. Series A, Math. Phys. Sci. 274 (1238), 45–53. http://www.jstor.org/stable/74329.
Testi, A., 2003. Alberi d'Italia. Giunti Editore, Firenze-Milano, p. 383.
Thivet, S., Gurioli, L., Di Muro, A., 2020. Basaltic dyke eruptions at Piton de La Fournaise: characterization of the eruptive products with implications for reservoir conditions, conduit processes and eruptive dynamics. Contrib. Mineral. Petrol. 175, 26. https://doi.org/10.1007/s00410-020-1664-5.
Vona, A., Romano, C., Dingwell, D.B., Giordano, D., 2011. The rheology of crystal-bearing basaltic magmas from Stromboli and Etna. Geochim. Cosmochim. Acta 75, 3214–3236.
Walker, G.P.L., 1967. Thickness and Viscosity of Etnean Lavas. Nature 213 (5075), 484–485. https://doi.org/10.1038/213484a0.
Walker, G.P.L., 1993. Basaltic-volcano systems. Geol. Soc. Lond., Spec. Publ. 76 (1), 3–38. https://doi.org/10.1144/GSL.SP.1993.076.01.01.